

Combined Experimental and Computational Investigation of the Elementary Reaction of Ground State Atomic Carbon ($C; ^3P_j$) with Pyridine ($C_5H_5N; X^1A_1$) via Ring Expansion and Ring Degradation Pathways

Michael Lucas, Aaron M. Thomas, and Ralf I. Kaiser*¹

Department of Chemistry, University of Hawai'i at Manoa, Honolulu, Hawaii 96822, United States

Eugene K. Bashkirov and Valeriy N. Azyazov

Samara University, Samara, 443086, Russia

Alexander M. Mebel*²

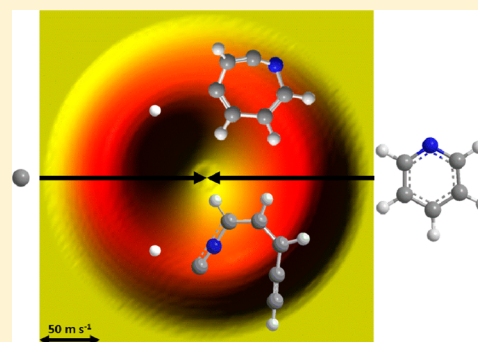
Department of Chemistry and Biochemistry, Florida International University, Miami, Florida 33199, United States

Samara University, Samara, 443086, Russia

Supporting Information

ABSTRACT: We explored the elementary reaction of atomic carbon ($C; ^3P_j$) with pyridine ($C_5H_5N; X^1A_1$) at a collision energy of 34 ± 4 kJ mol⁻¹ utilizing the crossed molecular beams technique. Forward-convolution fitting of the data was combined with high-level electronic structure calculations and statistical (RRKM) calculations on the triplet C_6H_5N potential energy surface (PES). These investigations reveal that the reaction dynamics are indirect and dominated by large range reactive impact parameters leading via barrier-less addition to the nitrogen atom and to two chemically nonequivalent “aromatic” carbon–carbon bonds forming three distinct collision complexes. At least two reaction pathways through atomic hydrogen loss were identified on the triplet surface. These channels involve multiple isomerization steps of the initial collision complexes via *ring-opening* and *ring expansion* forming an acyclic 1-ethynyl-3-isocyanoallyl radical (**P1**; $^2A''$) and a hitherto unreported seven-membered 1-aza-2-dehydrocyclohepta-2,4,6-trien-4-yl radical isomer (**P3**; 2A), respectively.

For RRKM calculations at zero collision energy, representing conditions in cold molecular clouds, the ring expansion product **P3** is formed nearly exclusively for the atomic hydrogen loss channel, but based on these computations, the molecular fragmentation channel forming acetylene (C_2H_2) plus 3-cyano-2-propen-1-ylidene (**P6**; $^3A''$) accounts for nearly all of the degradation products of the reaction of atomic carbon with pyridine, proposing a destruction pathway of interstellar pyridine, which may account for the absence in the detection of pyridine in the interstellar medium. These results are also discussed in light of the isoelectronic carbon–benzene ($C_6H_6; X^1A_1$) system with important implications to the rapid degradation of nitrogen-bearing polycyclic aromatic hydrocarbons (NPAHs) in the interstellar medium compared to mass growth processes of PAH counterparts through ring expansion.



1. INTRODUCTION

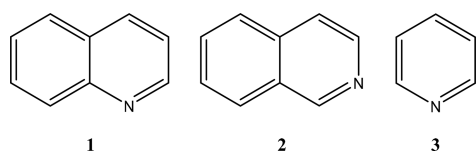
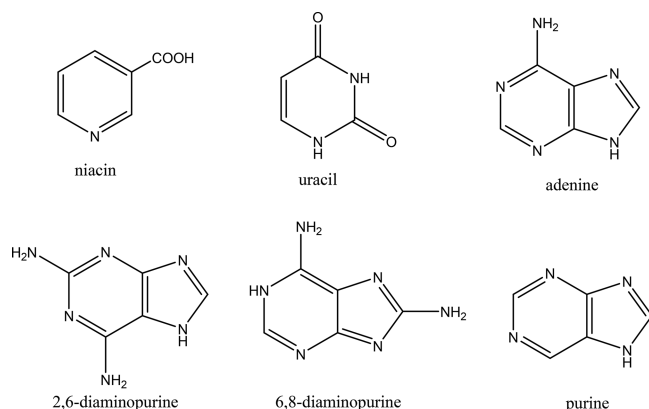
During the last decades, nitrogen-substituted polycyclic aromatic hydrocarbons (NPAHs) such as quinoline (**1**) and isoquinoline (**2**) (C_9H_7N) along with their simplest building block—the pyridine molecule (**3**) (C_5H_5N) (Scheme 1)—have received considerable attention since the discovery of vitamin B3 (niacin) and nucleobases (pyrimidines, purines) in carbonaceous chondrites such as Murchison (Scheme 2).^{1–4} The identification of the terrestrially rare nucleobases 2,6-diaminopurine and 6,8-diaminopurine in Murchison together with substantial D/H and ¹⁵N/¹⁴N isotope enrichments

propose extraterrestrial sources of their formation.³ NPAHs are linked to polycyclic aromatic hydrocarbons (PAHs) by formally replacing one or more methylidyne (CH) moieties by isoelectronic nitrogen atoms (N). Here, PAHs are likely formed via low- (cold molecular clouds; TMC-1) and high-temperature routes (circumstellar envelopes; IRC+10216); these pathways might lead to NPAHs in interstellar and circumstellar

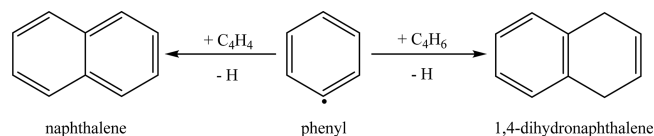
Received: January 23, 2018

Revised: March 5, 2018

Published: March 12, 2018

Scheme 1. Molecular Structures of Quinoline (1), Isoquinoline (2), and Pyridine (3)**Scheme 2. Molecular Structures of Niacin and Selected Nucleobases Identified in Murchison.³**

environments as well. In detail, the aforementioned reactions involve hydrogen-abstraction/acetylene-addition (HACA) type or vinylacetylene and 1,3-butadiene-mediated pathways, with the latter being barrierless proceeding even at temperatures as low as 10 K.^{5–12} These mechanisms are in strong analogy to barrier-less, rapid neutral–neutral reactions involving overall exoergic processes leading to a facile formation of (methyl-substituted) PAHs, which can be formally derived from naphthalene ($C_{10}H_8$)¹³ and 1,4-dihydronaphthalene ($C_{10}H_{10}$)¹⁴ upon reaction of phenyl-type radicals with vinylacetylene (C_4H_4 ; $H_2C=CH-C\dot{C}H$) and (methyl-substituted)^{7,15} 1,3-butadiene (C_4H_6 ; $H_2C=CH-CH=CH_2$) (Scheme 3). In these reactions, the chemical dynamics involve

Scheme 3. Formation of Naphthalene ($C_{10}H_8$) and 1,4-Dihydronaphthalene ($C_{10}H_{10}$) from the Reactions of the Phenyl Radical (C_6H_5) with Vinylacetylene (C_4H_4) and 1,3-Butadiene (C_4H_6), Respectively

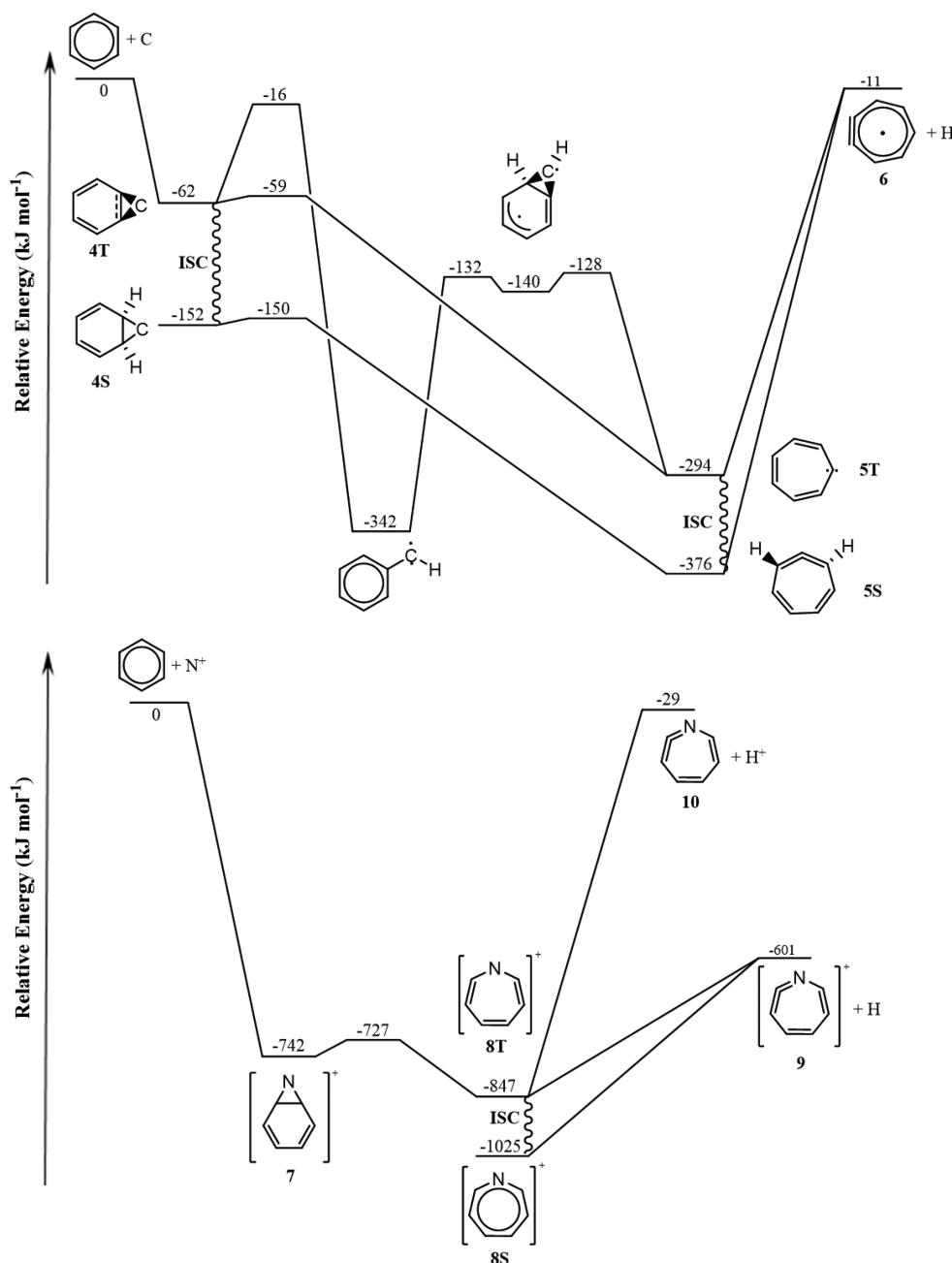
a defacto barrier-less addition of the phenyl-type radical within an initial van der Waals complex through a submerged barrier to a vinyl-type moiety (H_2CCR ($R = H, CH_3$)) yielding a resonantly stabilized free radical intermediate (RSFR).¹⁶ The latter isomerized yielding a cyclic intermediate, which then undergoes aromatization and PAH formation via atomic hydrogen loss.

However, even though the underlying formation mechanisms of NPAHs are beginning to emerge, little is known on the chemical reactivity of their simplest nitrogen-bearing building block: pyridine (C_5H_5N ; X^1A_1). This is in strong contrast to the isoelectronic benzene molecule—the building block of PAHs. The chemical dynamics of benzene (C_6H_6 ; X^1A_{1g}) reactions

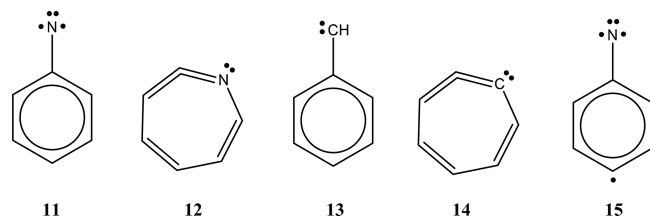
with important interstellar reactants such as carbon (C ; 3P_j),^{17,18} ethynyl (C_2H ; $^2\Sigma^+$),¹⁹ cyano (CN ; $^2\Sigma^+$),²⁰ and dicarbon (C_2 ; $^2\Sigma_g^+$)²¹ were explored on the microscopic level exploiting crossed molecular beams. Here, all reactions involve barrier-less additions of the open shell reactants followed by addition–elimination reactions in the case of ethynyl, cyano, and dicarbon. In the case of ground state atomic carbon, the reaction was more complex. The reaction is initiated by the barrierless addition of carbon to the π system of benzene forming a bicyclic intermediate (**4T**) followed by a ring expansion through C–C ring opening to a seven-membered ring intermediate (**5T**). This seven-membered ring intermediate, triplet cycloheptatrienylidene, decomposes through a loss of atomic hydrogen without an exit barrier to produce 1,2-didehydrocycloheptatrienyl radical (C_7H_5 ; X^2B_1 ; **6**) plus atomic hydrogen (Scheme 4).^{17,18} It should be noted that the reaction of singly ionized atomic nitrogen (N^+ ; 3P), which is isoelectronic to atomic carbon, with benzene (C_6H_6 ; X^1A_{1g}), has been explored experimentally and theoretically as well.^{22–25} The major product channel was the charge transfer process forming singly ionized benzene. Ascenzi et al. also monitored the formation of C–N containing species and observed H_2CN^+ , $H_2C_2N^+$, $H_2C_3N^+$, $H_3C_4N^+$, HC_5N^+ , and $H_2C_5N^+$.^{23,24} The N^+ ion was found to attack the π system of benzene without a barrier forming a bicyclic $C_6H_6N^+$ intermediate (**7**), which then underwent ring expansion via C–C bond fission forming a seven-member $C_6H_5N^+$ ring, the triplet azepine nitrenium cation (**8T**). This is similar to the isoelectronic carbon–benzene system, where atomic carbon added to the π system of benzene forming a bicyclic C_7H_6 intermediate (**4T**) followed by the ring expansion to the seven-member ring intermediate (**5T**) before losing atomic hydrogen forming C_7H_5 (**6**). Unlike C_7H_6 , (**8T**) depicts two competing dissociation pathways; it can eliminate a proton to form the neutral 1-azo-1,2,4,6-cycloheptatetraene, C_6H_5N (**10**), or it can lose a hydrogen atom to form the cation, $C_6H_5N^+$ (**9**). $C_6H_5N^+$ can also be formed after intersystem crossing (ISC) to the singlet azepine nitrenium cation (**8S**), which is 178 kJ mol^{−1} lower in energy than (**8T**).

Nevertheless, despite recent experimental and theoretical evidence of potential formation pathways of pyridine^{6,26–28} in interstellar and circumstellar environments, pyridine (C_5H_5N ; X^1A_1) has not been detected in extraterrestrial environments so far although the isoelectronic benzene molecule (C_6H_6 ; X^1A_{1g}) and its cyanobenzene derivative (C_6H_5CN ; X^1A_1),²⁹ which is formed via the barrier-less neutral–neutral reaction of benzene³⁰ with the cyano radical,²⁰ have been identified toward the planetary nebulae CRL618³¹ and molecular cloud TMC-1,²⁹ respectively. This calls for a systematic investigation of the underlying destruction pathways and hence chemical reactivity of pyridine with abundant reactants in the interstellar medium. Here, we explore the chemical dynamics of the reaction of pyridine with the simplest ubiquitous atomic reactant—ground state atomic carbon—under single collision conditions to unravel the hitherto unknown chemistry of gas phase pyridine via neutral–neutral reactions. These findings are then applied to propose a reaction and hence a destruction pathway of pyridine as well as pyridine-containing NPAHs in extraterrestrial environments. It should be stressed that only a little information is available on the C_6H_5N potential energy surface (PES) characterizing cyclic structures both experimentally and computationally. These studies mainly focused on the interconversion of phenylnitrene (**11**) and 1-azo-1,2,4,6-cycloheptatetraene (**12**) (Scheme 5).^{32–35} Phenylnitrene has

Scheme 4. Schematic Representation of the Potential Energy Surfaces of the Reactions of Ground State Carbon with Benzene (Top) and Singly Ionized Nitrogen with Benzene (Bottom) Based on the Calculations in Refs 17, 24, and 25



Scheme 5. Molecular Structures of Phenylnitrene (11), 1-Azo-1,2,4,6-cycloheptatetraene (12), Phenylcarbene (13), Cycloheptatetraene (14), and 4-Dehydrophenylnitrene (15)



a triplet ground state with triplet–singlet splitting of 63–75 kJ mol⁻¹.³⁶ On the other hand, the interconversion of (11) and (12) in the lowest singlet state is close to thermoneutral

allowing for rapid interconversion to occur at low temperatures.^{32–34} Phenylcarbene (13) has shown a distinct chemistry compared to phenylnitrene including a smaller triplet–singlet splitting of close to 10 kJ mol⁻¹ and a more exoergic reaction (also in the singlet state) to cycloheptatetraene (14) of about -86 kJ mol⁻¹.^{34,37}

The electronic structure of dehydrophenylnitrene (15) was calculated after the synthesis of 4-dehydro-2,3,5,6-tetrafluorophenylnitrene in a cryogenic matrix in its quartet ground state.^{38,39} The ground states of 4- and 2-dehydrophenylnitrene were calculated to be a quartet ground state, while the ground state of 3-dehydrophenylnitrene existed in a doublet ground state.³⁸ These high-spin molecules could have interest as molecular magnets as well as for synthetic and theoretical chemistry as these molecules contain both the phenylnitrene

and phenyl radical motifs. There have been no reports of a seven-membered C_6H_4N ring species. Here, we report on the crossed molecular beams reaction of ground state carbon (C ; 3P_j) with pyridine (C_5H_5N ; X^1A_1) to explore the hitherto elusive reaction dynamics of the pyridine molecule with atomic carbon leading to 1-aza-2-dehydrocyclohepta-2,4,6-trien-4-yl and 1-ethynyl-3-isocyanoallyl radicals via ring expansion and ring degradation pathways, respectively. These studies are combined with electronic structure calculations and compared to the isoelectronic carbon–benzene system investigated earlier to explore similarities, but also differences, of the underlying reaction dynamics.

2. EXPERIMENTAL AND THEORETICAL METHODS AND DATA ANALYSIS

2.1. Experiment. The gas phase reaction of atomic carbon (C ; 3P_j) with pyridine (C_5H_5N ; X^1A_1 ; Sigma-Aldrich; 99.8%+) was studied under single collision conditions in a crossed molecular beams machine.^{40–43} The supersonic carbon source has been previously reported in detail.^{44–50} Briefly, a pulsed molecular beam of helium-seeded carbon atoms was produced by ablating a rotating graphite rod by 266 nm photons from the output of a Nd:YAG laser (Quanta Ray Pro 270, Spectra Physics) operating at 30 Hz and power of 10–13 mJ per pulse. The ablated carbon was seeded in helium carrier gas (Airgas; 99.9999%) with a backing pressure of 4 atm released from a piezoelectric pulse valve operating at a repetition rate of 60 Hz, a pulse width of 80 μ s, and a peak voltage of -400 V. The pulsed carbon molecular beam passes through a skimmer and is velocity selected by a four-slot chopper wheel rotating at 120 Hz. The on-axis characterization of the pulsed carbon beam at m/z 12 (C^+) indicates a peak velocity (v_p) of 2644 ± 106 ms^{-1} and a speed ratio (S) of 3.3 ± 0.6 . The electronic states of the carbon molecular beam have been characterized previously, and at these velocities, atomic carbon is only in its 3P_j electronic ground state, but not in its 1D electronically excited state.^{44,51} The carbon beam is crossed perpendicularly with a pulsed argon (Airgas; 99.9999%) seeded pyridine beam at a seeding fraction of about 4% generated in the secondary source chamber by a piezoelectric pulse valve at a backing pressure of 550 Torr with a repetition rate of 60 Hz, a pulse width of 80 μ s, and a peak voltage of -400 V. The pyridine molecular beam was determined to have a v_p and S of 592 ± 20 ms^{-1} and 11.6 ± 0.4 yielding a collision energy (E_{col}) of 34 ± 4 $kJ mol^{-1}$ and a center-of-mass angle of $57 \pm 1^\circ$. The reactively scattered products were detected with a rotatable, triply differentially pumped, liquid nitrogen-cooled detection system. The neutral products are ionized with an electron impact ionizer at electron energy of 40 eV and an emission current of 1.2 mA and are mass-selected with a quadrupole mass spectrometer (QMS; Extrel QC 105); the ion flight constant (α) was determined to be 4.25 $\mu s amu^{-1/2}$ at these experimental conditions. The mass-selected ions are accelerated toward an aluminum coated stainless steel doorknob shaped target at -22.5 kV, initiating an electron cascade when an ion strikes the aluminum coated target and travels toward an organic scintillator to create a photon pulse that is further amplified by a photomultiplier tube (PMT; Burle Model 8850; -1.35 kV). A discriminator (Advanced Research Instruments Model F-100TD) at a level of 1.6 mV was used to filter the signal from the PMT before the TOF spectra are collected by a multichannel scaler (Stanford Research System SR430). The detector is rotatable within the

plane of the reactant beams. Up to 3×10^6 TOF spectra were recorded at each angle. The laboratory angular distribution was acquired by integration of the TOF spectra at each collection angle and normalizing for the accumulation time and fluctuations in the carbon beam intensity. The TOF data was converted from the laboratory frame to the center-of-mass (CM) frame by a forward-convolution routine to analyze the reaction dynamics and energetics.^{52,53} This approach initially presumes an angular flux distribution $T(\theta)$ and translational energy flux distribution $P(E_T)$ in the center-of-mass system assuming mutual independence. The laboratory data (TOF spectra and laboratory angular distribution) are then calculated from the $T(\theta)$ and $P(E_T)$ and convoluted over the apparatus functions to obtain a simulation of the experimental data. The crucial output of this fitting routine is the product flux contour map, $I(\theta, u) = P(u) \times T(\theta)$, which reports the intensity of the reactively scattered products (I) as a function of the center-of-mass scattering angle (θ) and product velocity (u). This plot is called the reactive differential cross section and can be seen as the image of the chemical reaction.

2.2. Theory. Geometries of all reactants, products, intermediates, and transition states involved in the reaction of ground state carbon atoms with pyridine occurring on the triplet C_6H_5N potential energy surfaces (PES) were optimized at the hybrid density functional B3LYP/6-311G** level of theory.^{54,55} Vibrational frequencies were computed at the same theoretical level and were utilized to evaluate zero-point vibrational energies (ZPE) and to calculate rate constants of unimolecular reaction steps of different C_6H_5N intermediates. The optimized Cartesian coordinates and vibrational frequencies are presented in Table S1. The connections between various reaction intermediates and transition states were verified by intrinsic reaction coordinate (IRC) calculations. Energies of various species were refined using explicitly correlated CCSD(T)-F12 calculations^{56,57} with the cc-pVTZ-f12 basis set,⁵⁸ which provide a close approximation for CCSD(T) energies at the complete basis set (CBS) limit. The expected accuracy of relative energies computed at the CCSD(T)-F12/cc-pVTZ-f12 level is within 5 $kJ mol^{-1}$,⁵⁹ if the wave function does not exhibit a strong multireference character. To ensure this, T1 diagnostics values from CCSD calculations were checked for every structure. The values appeared to be below 0.02–0.03 for all triplet C_6H_5N structures indicating that the CCSD(T)-F12 energies should be reliable. However, for several C_6H_4N isomers in a doublet electronic state, which represent potential H elimination products, the T1 diagnostics appeared to be high, pointing at a significant multireference character of their wave functions. Therefore, for relatively low-lying C_6H_4N structures, single-point energies were recalculated using the multireference second-order perturbation theory CASPT2 method^{60,61} with an active space including 10 electrons distributed on 10 orbitals, (10,10), and with the cc-pVTZ basis set. All the structures in question have a plane of symmetry and the active space included all electrons of the π -system (7), the lone pair of the nitrogen atom (2), and an unpaired σ -electron (1) distributed on 7 π and 3 σ orbitals. The B3LYP, CCSD(T)-F12, and CASPT2 quantum chemical calculations were performed using the GAUSSIAN 09⁶² and MOLPRO 2010⁶³ program packages. Rate constants of all unimolecular reaction steps on the triplet C_6H_5N PES accessed by the initial association of atomic carbon with pyridine were computed using Rice-Ramsperger-Kassel-Marcus (RRKM) theory,^{64–66} as functions of available internal

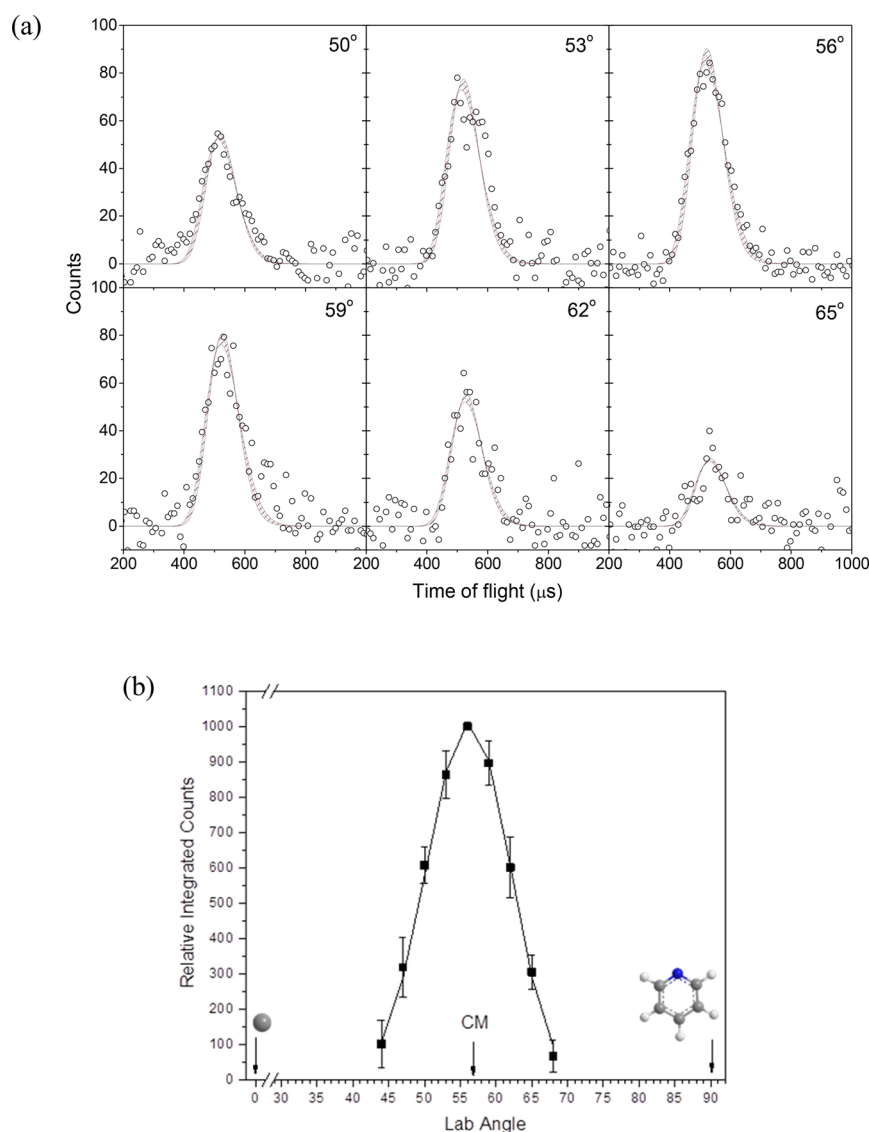


Figure 1. Time-of-flight data (a) and laboratory angular distribution (b) recorded at $m/z = 90$ ($C_6H_4N^+$) for the reaction of ground state atomic carbon (C) with pyridine (C_5H_5N) forming C_6H_4N product(s). The circles represent the experimental data, error bars represent the standard deviation, and the solid lines represent the fit.

energy of each intermediate or transition state, where numbers and densities of states were obtained within the harmonic approximation using B3LYP/6-311G** computed frequencies. The internal energy was taken as a sum of the collision energy and a negative of the relative energy of a species with respect to the reactants (the chemical activation energy). One energy level was considered throughout as at a zero-pressure limit closely corresponding to crossed molecular beam conditions. For H elimination channels on the triplet surface which were found to occur without an exit barrier, rate constants were computed using microcanonical variational transition state theory (VTST).^{64–66} Then, RRKM and VTST rate constants were utilized to compute product branching ratios by solving first-order kinetic equations within steady-state approximation. More detail on the ab initio/RRKM calculations can be found in our previous works.^{67,68}

3. RESULTS

3.1. Experimental Results. Reactive scattering signal from the reaction of atomic carbon (C; 3P ; 12 amu) with pyridine

(C_5H_5N ; X^1A_1 ; 79 amu) was monitored from $m/z = 91$ ($C_6H_5N^+$) to 88 ($C_6H_2N^+$). After scaling, the time-of-flight (TOF) spectra at these mass-to-charge ratios depicted identical patterns; therefore, these ions correspond to the ^{13}C substituted parent ($m/z = 91$), to the parent ion $C_6H_4N^+$ ($m/z = 90$), and to the most intense fragments ($m/z = 89$ and 88). Since $m/z = 90$ had the best signal-to-noise ratio, all laboratory data were recorded at this mass-to-charge ratio from 44° to 68° at steps of 3° (Figure 1). Note that the ablation of the graphite rod also produces dicarbon (C_2) and tricarbon (C_3) with the same velocity as atomic carbon.^{44,45} Tricarbon does not react with closed-shell hydrocarbons since these reactions are highly endoergic,^{68,69} this also holds for the reaction of tricarbon with pyridine, which does not show any reactive scattering signal at higher masses such as $m/z = 114$ ($C_8H_4N^+$). Dicarbon on the other hand undergoes barrier-less, exoergic reactions with unsaturated hydrocarbons via atomic hydrogen elimination and expansion of the carbon skeleton by two carbon atoms.^{21,68} However, the dicarbon concentration in the present molecular beam is very low and only about 5% compared to atomic

carbon. No signal from the dicarbon–pyridine reaction could be observed such as at $m/z = 112$ ($C_7H_4N^+$); consequently, we can conclude that dissociative ionization of higher molecular mass products does not contribute to the signal to $m/z = 90$. The resulting laboratory angular distribution is nearly forward–backward symmetric; this finding suggests indirect scattering dynamics via the formation of a long-lived C_6H_5N complex, which fragments via atomic hydrogen loss to form the C_6H_4N product(s). To gauge the relative reaction cross section with respect to atomic hydrogen loss of the carbon–pyridine system compared to the reaction of ground state carbon atoms with benzene, the latter system was reinvestigated^{17,18} under identical primary source conditions with a benzene beam in the secondary source. Overall, accounting for the distinct vapor pressures of benzene (75 Torr) and pyridine (16 Torr) at 293 K, the reactive scattering signal of the carbon–benzene system was a factor of 2 higher than the carbon–pyridine system, which is indicative of a larger reactive cross section of carbon reacting with benzene compared to pyridine in case of the atomic hydrogen loss channel.

To derive information on the reaction dynamics and underlying mechanism, the TOF data and laboratory angular distribution were converted from the laboratory frame to the center-of-mass reference frame exploiting a forward convolution routine (Section 2). Figure 2 displays the resulting center-of-mass translational energy distribution ($P(E_T)$) and the angular flux distribution ($T(\theta)$). The laboratory data (Figure 1) could be fit with a single product channel of the product mass combination of 90 amu (C_6H_4N) plus 1 amu (H). The $P(E_T)$ extends to a maximum energy of 68 ± 15 kJ mol⁻¹; for those products born without internal excitation, the maximum energy release represents the sum of the reaction exoergicity plus the collision energy ($E_{col} = 34 \pm 4$ kJ mol⁻¹) (Figure 2a). Therefore, subtracting the collision energy from the maximum translational energy suggests that the reaction of a ground state carbon atom with pyridine to form C_6H_4N plus atomic hydrogen is exoergic by 34 ± 19 kJ mol⁻¹. Further, the $P(E_T)$ displays a broad plateau ranging from zero to 15 kJ mol⁻¹; this finding indicates multiple exit channels of which at least one is rather loose when the C_6H_5N intermediate(s) decomposes to C_6H_4N plus atomic hydrogen.^{21,47,49,70,71} Also, the center-of-mass angular distribution $T(\theta)$ (Figure 2b) shows intensity across the complete angular range from 0° to 180° with a forward–backward symmetric scattering pattern suggesting indirect scattering dynamics via a long-lived C_6H_5N intermediate. The lifetime of the complex is longer than its rotational period. Finally, the $T(\theta)$ has a minimum at 90° indicating geometric constraints on the decomposition of the C_6H_5N complex where the hydrogen atom is ejected in the plane of the decomposing complex and hence perpendicularly to the total angular momentum vector. The overall rather poor polarization of the angular distribution is a direct result of the inability of the light hydrogen atom to carry away significant angular momentum, which leads to an inefficient coupling between the initial and final orbital angular momentum. The associated product flux map, $I(\theta, v) = P(v) \times T(\theta)$, for the reaction of ground-state carbon atom $C(^3P_j)$ and pyridine, reports the intensity of the reactively scattered products (I) as a function of the center-of-mass scattering angle (θ) and product velocity (v).

3.2. Computational Results. The computations at the CCSD(T)-F12/cc-pVTZ-f12//B3LYP/6-311G** + ZPE-(B3LYP/6-311G**) level of theory reveal five energetically

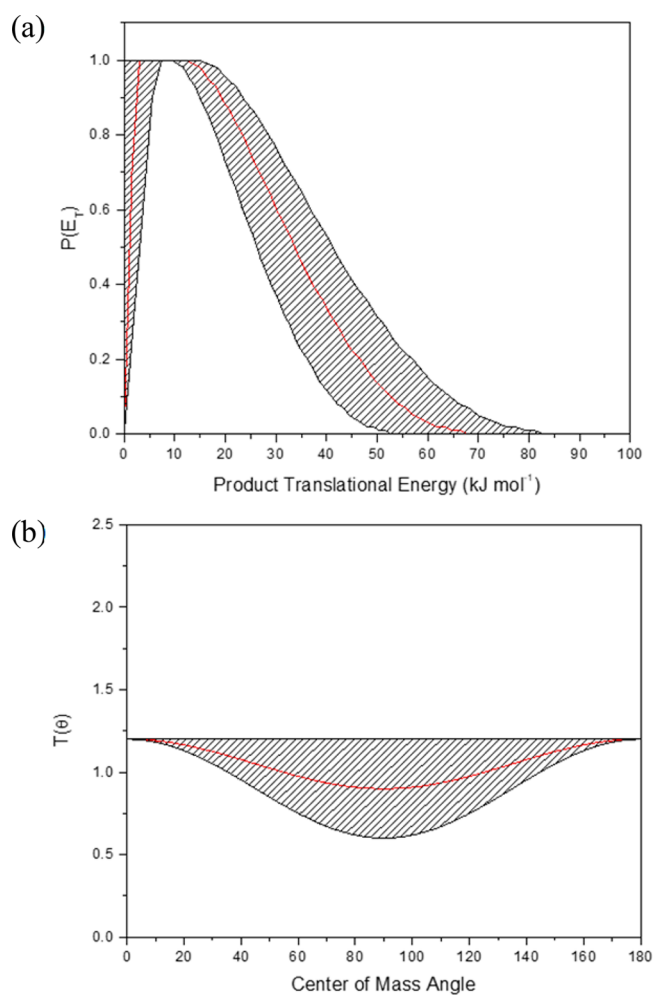


Figure 2. Center-of-mass translational energy flux distribution $P(E_T)$ (a) and angular distribution $T(\theta)$ (b) for the atomic hydrogen loss channel in the reaction of carbon with pyridine forming C_6H_4N product(s). Hatched areas indicate the acceptable upper and lower error limits of the fits and solid red lines define the best-fit functions.

accessible atomic hydrogen loss product channels (P1–P5) as well as an acetylene (C_2H_2) plus 3-cyano-2-propen-1-ylidene (CHCHCHCN) pathway (P6) with the hydrogen loss being thermoneutral to weakly exoergic by only up to 29 kJ mol⁻¹ compared to the molecular dissociation pathway (-113 kJ mol⁻¹) (Figure 3). Note that many other higher in energy C_6H_4N isomers may exist with either doublet or quartet being the ground electronic states; their relative energies, electronic terms, and relation to C_6H_5N intermediates are illustrated in Figures S1 and S2 in the Supporting Information. Our computations reveal the existence of three barrier-less entrance channels via addition to the nitrogen atom (i1) and to two chemically nonequivalent “aromatic” carbon–carbon bonds $C2=C3$ and $C5=C6$ forming i2 and i3, respectively, on the triplet surface. The initial collision complexes isomerize via multiple pathways that eventually lead to dissociative product channels forming P1–P6. The lowest energy product channel involves a molecular decomposition pathway yielding acetylene (C_2H_2) plus 3-cyano-2-propen-1-ylidene (CHCHCHCN) (P6). Starting from collision complex, i1 isomerizes to the seven-membered cyclic intermediate i7 through a defacto atomic carbon insertion into the carbon–nitrogen bond of pyridine. Alternatively, intermediate i7 can be accessed via i8

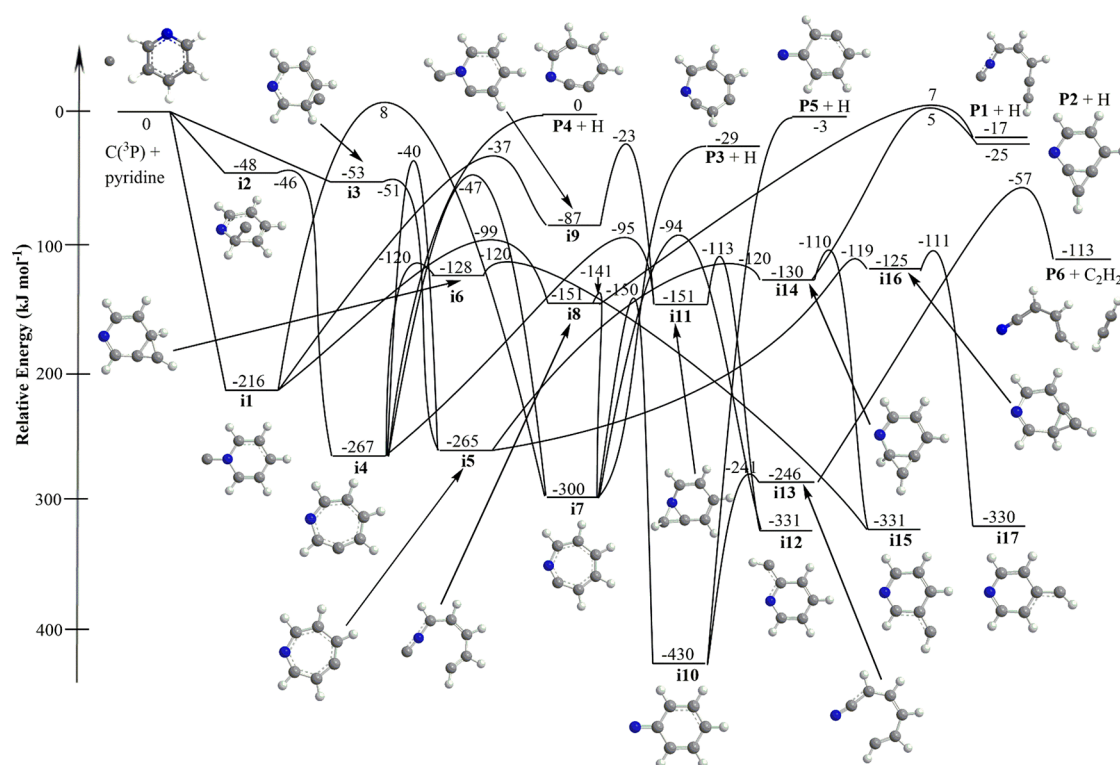


Figure 3. Potential energy surface for the reaction of ground state carbon (C ; 3P) plus pyridine (C_5H_5N ; X^1A_1). The energies of intermediates and transition states relative to the separated reactants are given in kJ mol^{-1} as calculated at the CCSD(T)-F12/cc-pVTZ-f12//B3LYP/6-311G** + ZPE(B3LYP/6-311G**) level of theory. Optimized Cartesian coordinates are compiled in the [Supporting Information](#).

through ring opening–ring closure processes. Note that the formation of **i7** is also feasible via ring opening in **i2** to **i4** followed by hydrogen shift. Finally, **i3** can also ring open to **i5** which then undergoes a hydrogen migration to **i4**. Therefore, all three initial collision complexes can lead to **i7**. Overall, **i7** isomerizes to phenylnitrene (**i10**), which represents the global minimum of the triplet surface stabilized by 430 kJ mol^{-1} , with respect to the separated reactants. This intermediate isomerizes via ring opening to **i13**, which then undergoes unimolecular decomposition via a tight transition state involving a C–C bond fission forming acetylene (C_2H_2) plus 3-cyano-2-propen-1-ylidene (CHCHCHCN) (**P6**).

The five hydrogen atom loss channels (**P1**–**P5**), of which three are barrier-less (**P3**–**P5**), are much less exoergic compared to the acetylene channel (**P6**). The overall most exoergic pathway to **P3** (1-aza-2-dehydrocyclohepta-2,4,6-trien-4-yl) holds an exoergic of -29 kJ mol^{-1} and occurs through the loss of atomic hydrogen at C3 of **i7**. Another seven-membered cyclic product **P4** is nearly isoergic to the reactants and forms via hydrogen loss from C2 of intermediate **i4**. Whereas the formation of the six-membered cyclic product **P5** occurs through atomic hydrogen loss from **i10** and is slightly exoergic by 3 kJ mol^{-1} , the remaining product channels (**P1** and **P2**) hold tight transition states that lie well above the separated reactants by 26 and 30 kJ mol^{-1} , respectively. The acyclic product **P1** is formed via hydrogen loss from the acyclic intermediate **i8**, while the exotic bicyclic product **P2** involves a C–C ring closure to form the bicyclic intermediate **i14**, which in turn is connected to **i5**.

In addition to these dissociation pathways, we identified low lying reaction intermediates (**i12**, **i15**, **i17**), which are linked to overall highly endoergic dissociation pathways and are

energetically closed in our experiment ([Supporting Information](#)). The pyridylmethylene intermediates **i12** (2-pyridylmethylene), **i15** (3-pyridylmethylene), and **i17** (4-pyridylmethylene) have similar stabilities within 1 kJ mol^{-1} . **i17** is formed from **i5** through intermediate **i16** (3-azabicyclo[4.1.0]hepta-2,4,6-triene) that originates from a C3–C5 ring closure followed by a ring opening. There are two pathways that support formation of **i15** both including a C–C ring opening bond fission from the bicyclic intermediates **i6** and **i14**. **i12** can form from the isomerization of **i7** and can be accessed from a C–N ring opening bond fission from the bicyclic intermediate **i11**. The bicyclic intermediate **i11** can be formed by a C–N ring closing bond fusion from **i4** or from **i1** through a higher energy pathway that involves a 1,3-hydrogen shift to form **i9** followed by a C–C ring closure.

Finally, we exploited statistical calculations to predict the branching ratios computationally at the collision energy of 34 kJ mol^{-1} and also within the limits approaching 0 kJ mol^{-1} representing conditions in cold molecular clouds ([Table 1](#)). [Table 1](#) is divided into two reaction pathways originating from the initial collision complex **i1** and from the collision complexes **i2** and **i3**. These computations reveal that the reaction of pyridine with atomic carbon is dominated by destruction leading via acetylene loss to 3-cyano-2-propen-1-ylidene (CHCHCHCN). The atomic hydrogen loss was found to be only a minor pathway with branching ratios **P1**:**P2**:**P3**:**P4**:**P5** for the **i2**/**i3** pathway computed as 7.86:6.52:30.47:53.85:1.31 and for the **i1** pathway 19.86:0.16:75.41:1.33:3.24. Therefore, the **i1** pathway is dominated by the formation of **P3** with a yield of 75.41% of the hydrogen atom loss product, whereas the **P4** product channel represents the major product of the **i2**/**i3** pathway with slightly over half of the yield (53.85%) and with

Table 1. Calculated Branching Ratios of the C(³P) + Pyridine Reaction

	From i1		From i2 or i3	
	Total Yield	H Loss Only	Total Yield	H Loss Only
$E_{\text{col}} = 34 \text{ kJ mol}^{-1}$				
C ₂ H ₂ Loss	99.9979		99.9947	
P1	0.00042384	19.86%	0.00041511	7.86%
P2	3.4449×10^{-6}	0.16%	0.00034421	6.52%
P3	0.0016094	75.41%	0.00160935	30.47%
P4	2.8464×10^{-5}	1.33%	0.00284402	53.85%
P5	6.913×10^{-5}	3.24%	6.128×10^{-5}	1.31%
$E_{\text{col}} = 0 \text{ kJ mol}^{-1}$				
C ₂ H ₂ Loss	99.9997		99.9997	
P1	4.26×10^{-9}	0.00%	4.24×10^{-9}	0.00%
P2	6.6×10^{-9}	0.00%	2.35×10^{-7}	0.09%
P3	0.000266	99.69%	0.000266	99.61%
P4	0	0.00%	0	0.00%
P5	8.06×10^{-7}	0.30%	8.06×10^{-7}	0.30%

the P3 channel showing a contribution of 30.47%. Note that the statistical treatment predicts that P1 is formed to about 20% from i1. In the limit of zero collision energy, C₂H₂ elimination still represents the predominant reaction channel, but among the H loss channels the formation of P3 becomes nearly exclusive (99.6–99.7%, Table 1) regardless of the initial collision complex, with another slightly exoergic channel producing P5 giving a minor contribution; whereas the channel to P1 is then closed due to the exit barrier above the initial reactants.

4. DISCUSSION

We can now merge the experimental with the computational results to gain a detailed understanding of the underlying reaction dynamics of the ground state carbon–pyridine system. Let us consider the energetics of the reaction first. For this, we compare the calculated reaction energies leading to P1–P5 with the experimentally determined reaction energy of $-34 \pm 19 \text{ kJ mol}^{-1}$; hence, based on these energetics, at least P1–P3 hold overall reaction energies that fall within the range of the experimentally determined exoergic of $-34 \pm 19 \text{ kJ mol}^{-1}$. Note that these data do not exclude the formation of P4 and/or P5, which might be masked in the low energy section of the translational energy distribution. To elucidate the (dominating) reaction products, we will have a closer look at the peaking of the center-of-mass translational energy and angular distributions. First, recall that the $P(E_T)$ is characterized by a broad plateau from zero to about 15 kJ mol^{-1} , which is indicative of multiple exit channels in which at least one transition state is very loose, and a second transition state has a small exit barrier.

Therefore, this finding may suggest the formation of P3, P4, and/or P5 (barrierless decomposition) along with P1 and/or P2 (exit barrier of 26 and 30 kJ mol^{-1} , respectively). Considering the overall energetics of the reaction, we may conclude that at least P3 accounts for the barrierless pathway, whereas P1 and/or P2 contributes to the “off zero” peaking of the center of mass translational energy distribution. Once again, these data do not exclude the formation of P4 and/or P5, which might be linked to the barrierless decomposition pathways.

Can we narrow down these possibilities even further? Recall that a close inspection of the center-of-mass angular distribution reveals that the hydrogen atom must be emitted within the plane of the decomposing intermediate(s). The geometries of the (variational) transition states involved in the formation of P1 to P5 are shown in Figure 4 highlighting the direction and angle of the leaving hydrogen atom. The center-of-mass angular distribution is forward–backward symmetric and dips at 90°. Therefore, the hydrogen atom is eliminated within the plane of the decomposing complex. Product P2 can be easily eliminated as a major contributor since the transition state connecting i14 and P2 reveals a hydrogen atom ejected nearly perpendicularly to the plane of the decomposing complex at an angle of 70.8°, but not in plane as required. This conclusion also gains support from our RRKM calculations revealing only minor contributions of P2. Consequently, since P1 and P2 have been the sole candidates for an off-zero contribution to the center-of-mass translational energy distribution and P2 has been eliminated based on the geometrical constraints, P1 represents the (dominating) contributor to account for the off-zero peaking of the center-of-mass translational energy distribution. The inherent geometry of the transition state (Figure 4) support this conclusion documenting an emission of the hydrogen atom at about 26.0° with respect to the molecular plane, in which the carbon atom changes from an sp² in i8 to an sp hybridization in P1 on the ³A surface. Finally, product P3 accounts for the energetics of the reaction as derived experimentally, close to zero translational energy requirement for the hitherto missing barrierless reaction pathway, and for the geometrical constraints involved in the hydrogen loss relatively close to the former molecular plane in i7 (55.0°), which however becomes distorted along the H loss pathway, as P3 itself is nonplanar (Figure 4). Recall that the RRKM calculations predicted P3 to be the dominating and second most important product if the reaction proceeds via intermediates i1 and i2/i3, respectively. Considering P4 and P5, the hydrogen atoms are eliminated within the molecular plane (at 0°).

In summary, we conclude that at least two exit channels exist leading to the formation of the acyclic isomer 1-ethynyl-3-

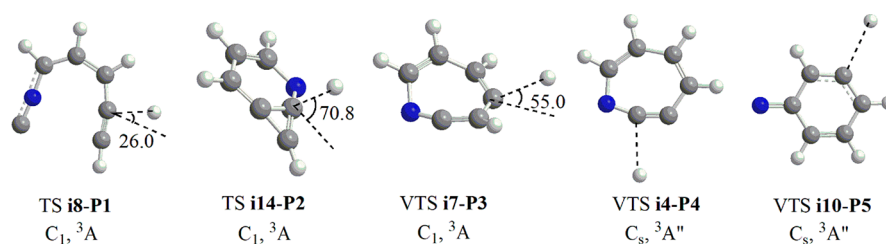


Figure 4. (Variational) transition states involved in the formation of five C₆H₄N isomers (P1–P5). The angle of the departing hydrogen atom is shown in degrees.

isocyanoallyl radical (P1) via a tight exit transition state involving *ring-opening* and to the cyclic 1-aza-2-dehydrocyclohepta-2,4,6-trien-4-yl radical isomer (P3) via a *defacto ring expansion* through a loose exit transition state along with the loss of atomic hydrogen within the plane of the fragmenting intermediates. Based on the experimental data alone, the formation of P4 and P5 cannot be excluded; RRKM calculations, however, agree that P5 represents only a minor contributor, whereas the yields of P4 depend critically on the initially formed intermediates, i.e., i1 versus i2/i3. Overall, the formation of P1 and P3 involves at least two (i1 → i8 → P1 + H; i2 → i4 → i7 → i8 → P1 + H; i3 → i5 → i4 → i7 → i8 → P1 + H) and three (i1 → i8 → i7 → P3 + H; i2 → i4 → i7 → P3 + H; i3 → i5 → i4 → i7 → P3 + H) reaction intermediates initiated by barrierless additions of atomic carbon to i1–i3.

Having elucidated the reaction mechanism of the reaction of atomic carbon with pyridine, we can compare these findings with the isoelectronic carbon–benzene surface. First, both reactions are initiated by a barrier-less addition to the carbon atom to the benzene/pyridine reactant on the triplet surface and involve indirect scattering dynamics via long-lived reaction intermediates. The reaction with pyridine was found to be more exoergic $-34 \pm 15 \text{ kJ mol}^{-1}$ compared to the carbon–benzene system yielding a reaction energy of only $-12 \pm 4 \text{ kJ mol}^{-1}$.¹⁷ Whereas the dynamics of the carbon–pyridine system are dictated at least by two distinct reaction mechanisms involving ultimately *ring-opening* (P1) and *ring expansion* (P3) plus atomic hydrogen, the carbon–benzene system exclusively undergoes ring expansion to a seven-membered 1,2-didehydrocycloheptatrienyl radical (C₇H₅; 6; X²B₁). Therefore, one of the noticeable differences in the chemical dynamics of the reactions of carbon with pyridine and benzene is that the bicyclic intermediates i11, i14, and i16 in the reaction with pyridine play no significant role.

While the reaction of atomic carbon and pyridine occurs on the triplet surface, it is unlikely for the singlet surface to be important to the reaction even though intersystem crossing (ISC) to the singlet PES is in principle possible in the vicinity of the carbene-type intermediates i12, i15, and i17. ISC was only found to play an important role for the reaction of carbon and acetylene, which leads to the formation of the C₃(X¹Σ_g⁺) + H₂ products.⁶⁸ This unique behavior was attributed to a relative long lifetime of the decomposing C₃H₂ complexes caused by the nearly thermoneutral or slightly exoergic triplet surface products *c*- and *l*-C₃H and these relatively long lifetimes allow for the triplet-singlet ISC to occur. The reaction of carbon and benzene may also have ISC play a role in the reaction but only in bulk conditions and not in the gas phase molecular beam experiments.⁶⁸

The most important results of the calculated branching ratios are how dominant the acetylene loss channel (P6) is (Table 1). The acetylene loss channel accounts for 99.9979% of the total yield at the present experimental conditions and 99.9997% of the total yield at zero collision energy. This result at zero collision energy represents the condition in interstellar clouds and provides an important insight into interstellar pyridine. Currently pyridine has not been detected in the interstellar medium. These results suggest that the reaction of atomic carbon with pyridine destroys pyridine into smaller fragments leading to the lack of interstellar pyridine to be detected. Note that the molecular decomposition pathway involving acetylene could not be probed in our experimental studies due to the inherent background from dissociative ionization of the

pyridine reactant fragmenting to the 3-cyano-2-propen-1-ylidene and acetylene products (P6).

5. CONCLUSIONS

The reaction of atomic carbon (C; ³P_i) with pyridine (C₅H₅N; X¹A₁) was investigated at an average collision energy of $34 \pm 4 \text{ kJ mol}^{-1}$ exploiting the crossed molecular beams technique. Forward-convolution fitting of the data was combined with high-level electronic structure calculations and statistical (RRKM) calculations on the triplet C₆H₅N potential energy surface (PES). These investigations suggest that the chemical reaction dynamics are indirect and dominated by large range reactive impact parameters leading via barrier-less addition reactions to three distinct collision complexes (i1–i3). At least two major reaction pathways were identified on the triplet surface which *de facto* involve multiple isomerization steps of the initial collision complexes via *ring-opening* and *ring expansion* forming the acyclic 1-ethynyl-3-isocyanoallyl (P1; ²A^o) and the previously unreported seven-membered 1-aza-2-dehydrocyclohepta-2,4,6-trien-4-yl isomer (P3; ²A), respectively, along with atomic hydrogen, via essentially lose exit transition states from long-lived triplet C₆H₅N intermediates. Based on the computations, the molecular fragmentation channel eliminating acetylene (C₂H₂) plays the most important role the reaction of atomic carbon with pyridine suggesting a possible destruction pathway of pyridine hitherto unobserved in the interstellar medium (ISM). Pyridine, a prototype six-member ring containing one N atom, is less stable than benzene; the aromatic stabilization energy of the former being 151 kJ mol^{-1} lower than that of the latter.⁷² Our studies also suggest that upon reaction with interstellar quinoline (1) and isoquinoline (2), reactions with atomic carbon lead to *ring expansion* (seven membered carbon based cyclic moiety) once carbon reacts with the benzene moiety, but predominantly to pyridine ring degradation if atomic carbon adds initially to the pyridine moiety of (iso)quinoline in low temperature interstellar environments. Therefore, the substitution of a methylidyne (CH) group by atomic nitrogen in PAHs leading to NPAHs is predicted to hold a profound effect on molecular mass growth processes as highly reactive carbon atoms might react with NPAHs essentially delimiting molecular mass growth in the interstellar medium.

■ ASSOCIATED CONTENT

📄 Supporting Information

The Supporting Information is available free of charge on the ACS Publications website at DOI: 10.1021/acs.jpca.8b00756.

Figure S1, optimized structures, electronic states, and relative energies (kJ mol⁻¹) of various H loss products originating from seven-member ring C₆H₅N isomers; Figure S2, optimized structures, electronic states, and relative energies (kJ mol⁻¹) of various H loss products originating from six-member ring C₆H₅N isomers; Table S1, optimized Cartesian coordinates (Å) and vibrational frequencies (cm⁻¹) for intermediates, transition states, dissociation products (PDF)

■ AUTHOR INFORMATION

Corresponding Authors

*E-mail: ralfk@hawaii.edu.

*E-mail: mebala@fiu.edu.

ORCID 

Ralf I. Kaiser: 0000-0002-7233-7206

Alexander M. Mebel: 0000-0002-7233-3133

Notes

The authors declare no competing financial interest.

ACKNOWLEDGMENTS

This work was supported by the US Department of Energy, Basic Energy Sciences DE-FG02-03ER15411 and DE-FG02-04ER15570 to the University of Hawaii and to Florida International University, respectively. The work at Samara University on ab initio calculations of the C + pyridine PES was supported by the Ministry of Education and Science of the Russian Federation under Grant No. 14.Y26.31.0020.

REFERENCES

- (1) Pizzarello, S.; Huang, Y.; Fuller, M. The Carbon Isotopic Distribution of Murchison Amino Acids. *Geochim. Cosmochim. Acta* **2004**, *68*, 4963–4969.
- (2) Pizzarello, S.; Huang, Y. The Deuterium Enrichment of Individual Amino Acids in Carbonaceous Meteorites: A Case for the Pre-Solar Distribution of Biomolecule Precursors. *Geochim. Cosmochim. Acta* **2005**, *69*, 599–605.
- (3) Callahan, M. P.; Smith, K. E.; Cleaves, H. J., II; Ruzicka, J.; Stern, J. C.; Glavin, D. P.; House, C. H.; Dworkin, J. R. Carbonaceous Meteorites Contain a Wide Range of Extraterrestrial Nucleobases. *Proc. Natl. Acad. Sci. U. S. A.* **2011**, *108*, 13995–13998.
- (4) Martins, Z.; Botta, O.; Fogel, M. L.; Sephton, M. A.; Glavin, D. P.; Watson, J. S.; Dworkin, J. P.; Schwartz, A. W.; Ehrenfreund, P. Extraterrestrial Nucleobases in the Murchison Meteorite. *Earth Planet. Sci. Lett.* **2008**, *270*, 130–136.
- (5) Parker, D. S. N.; Yang, T.; Dangi, B. B.; Kaiser, R. I.; Bera, P. P.; Lee, T. J. Low Temperature Formation of Nitrogen-Substituted Polycyclic Aromatic Hydrocarbons (PANHs) -Barrierless Routes to Dihydro(iso)quinolines. *Astrophys. J.* **2015**, *815*, 115.
- (6) Parker, D. S. N.; Kaiser, R. I. On the Formation of Nitrogen-Substituted Polycyclic Aromatic Hydrocarbons (NPAHs) in Circumstellar and Interstellar Environments. *Chem. Soc. Rev.* **2017**, *46*, 452–463.
- (7) Yang, T.; Muzangwa, L.; Kaiser, R. I.; Jamal, A.; Morokuma, K. A Combined Crossed Molecular Beam and Theoretical Investigation of the Reaction of the meta-Tolyl Radical with Vinylacetylene - Toward the Formation of Methylanthalenes. *Phys. Chem. Chem. Phys.* **2015**, *17*, 21564–21575.
- (8) Parker, D. S. N.; Kaiser, R. I.; Troy, T. P.; Ahmed, M. Hydrogen Abstraction-Acetylene Addition Revealed. *Angew. Chem., Int. Ed.* **2014**, *53*, 7740–7744.
- (9) Yang, T.; Troy, T. P.; Xu, B.; Kostko, O.; Ahmed, M.; Mebel, A. M.; Kaiser, R. I. Hydrogen-Abstraction/Acetylene-Addition Exposed. *Angew. Chem., Int. Ed.* **2016**, *55*, 14983–14987.
- (10) Golan, A.; Ahmed, M.; Mebel, A. M.; Kaiser, R. I. A VUV Photoionization Study of the Multichannel Reaction of Phenyl Radicals with 1,3-Butadiene under Combustion Relevant Conditions. *Phys. Chem. Chem. Phys.* **2013**, *15*, 341–347.
- (11) Frenklach, M. Reaction Mechanism of Soot Formation in Flames. *Phys. Chem. Chem. Phys.* **2002**, *4*, 2028–2037.
- (12) Kislov, V. V.; Islamova, N. I.; Kolker, A. M.; Lin, S. H.; Mebel, A. M. Hydrogen Abstraction Acetylene Addition and Diels-Alder Mechanisms of PAH Formation: A Detailed Study Using First Principles Calculations. *J. Chem. Theory Comput.* **2005**, *1*, 908–924.
- (13) Parker, D. S. N.; Zhang, F.; Kim, Y. S.; Kaiser, R. I.; Landera, A.; Kislov, V. V.; Mebel, A. M.; Tielens, A. G. G. M. Low Temperature Formation of Naphthalene and its Role in the Synthesis of PAHs (Polycyclic Aromatic Hydrocarbons) in the Interstellar Medium. *Proc. Natl. Acad. Sci. U. S. A.* **2012**, *109*, 53–58.
- (14) Kaiser, R. I.; Parker, D. S. N.; Zhang, F.; Landera, A.; Kislov, V. V.; Mebel, A. M. PAH Formation under Single Collision Conditions: Reaction of Phenyl Radical and 1,3-Butadiene to Form 1,4-Dihydronaphthalene. *J. Phys. Chem. A* **2012**, *116*, 4248–4258.
- (15) Parker, D. S. N.; Dangi, B. B.; Kaiser, R. I.; Jamal, A.; Ryazantsev, M. N.; Morokuma, K.; Korte, A.; Sander, W. An Experimental and Theoretical Study on the Formation of 2-Methylnaphthalene (C₁₁H₁₀/C₁₁H₉D₇) in the Reactions of the Para-Tolyl (C₇H₇) and Para-Tolyl-d₇ (C₇D₇) with Vinylacetylene (C₄H₄). *J. Phys. Chem. A* **2014**, *118*, 2709–2718.
- (16) Kaiser, R. I.; Parker, D. S. N.; Mebel, A. M. Reaction Dynamics in Astrochemistry: Low-Temperature Pathways to Polycyclic Aromatic Hydrocarbons in the Interstellar Medium. *Annu. Rev. Phys. Chem.* **2015**, *66*, 43–67.
- (17) Hahndorf, I.; Lee, Y. T.; Kaiser, R. I.; Vereecken, L.; Peeters, J.; Bettinger, H. F.; Schreiner, P. R.; Schleyer, P. v. R.; Allen, W. D.; Schaefer, H. F., III A Combined Crossed-Beam, Ab Initio, and Rice-Ramsperger-Kassel-Marcus Investigation of the Reaction of Carbon Atoms C(³P_j) with Benzene, C₆H₆(X ¹A_{1g}) and d₆-Benzene, C₆D₆(X ¹A_{1g}). *J. Chem. Phys.* **2002**, *116*, 3248–3262.
- (18) Kaiser, R. I.; Hahndorf, I.; Huang, L. C. L.; Lee, Y. T.; Bettinger, H. F.; Schleyer, P. v. R.; Schaefer, H. F., III; Schreiner, P. R. Crossed Beams Reaction of Atomic Carbon, C(³P_j), with d₆-Benzene, C₆D₆(X ¹A_{1g}): Observation of the Per-Deutero-1,2-Didehydro-Cycloheptatrienyl Radical, C₇D₅(X ²B₂). *J. Chem. Phys.* **1999**, *110*, 6091–6094.
- (19) Jones, B.; Zhang, F.; Maksyutenko, P.; Mebel, A. M.; Kaiser, R. I. Crossed Molecular Beam Study on the Formation of Phenylacetylene and Its Relevance to Titan's Atmosphere. *J. Phys. Chem. A* **2010**, *114*, 5256–5262.
- (20) Balucani, N.; Asvany, O.; Chang, A. H. H.; Lin, S. H.; Lee, Y. T.; Kaiser, R. I.; Bettinger, H. F.; Schleyer, P. v. R.; Schaefer, H. F., III Crossed Beam Reaction of Cyano Radicals with Hydrocarbon Molecules. I. Chemical Dynamics of Cyanobenzene (C₆H₅CN; X ¹A₁) and Perdeutero Cyanobenzene (C₆D₅CN; X ¹A₁) Formation from Reaction of CN(X ²Σ⁺) with Benzene C₆H₆(X ¹A_{1g}), and d₆-Benzene C₆D₆(X ¹A_{1g}). *J. Chem. Phys.* **1999**, *111*, 7457–7471.
- (21) Gu, X.; Guo, Y.; Zhang, F.; Mebel, A. M.; Kaiser, R. I. A Crossed Molecular Beams Study of the Reaction of Dicarboxyl Molecules with Benzene. *Chem. Phys. Lett.* **2007**, *436*, 7–14.
- (22) Arnold, S. T.; Williams, S.; Dotan, I.; Midey, A. J.; Morris, R. A.; Viggiano, A. A. Flow Tube Studies of Benzene Charge Transfer Reactions from 250 to 1400 K. *J. Phys. Chem. A* **1999**, *103*, 8421–8432.
- (23) Ascenzi, D.; Franceschi, P.; Freearge, T. G. M.; Tosi, P.; Bassi, D. C-N Bond Formation in the Reaction of Nitrogen Ions N⁺ with Benzene Molecules. *Chem. Phys. Lett.* **2001**, *346*, 35–40.
- (24) Di Stefano, M.; Rosi, M.; Sgamellotti, A.; Ascenzi, D.; Bassi, D.; Franceschi, P.; Tosi, P. Experimental and Theoretical Investigation of the Production of Cations Containing C-N Bonds in the Reaction of Benzene with Atomic Nitrogen Ions. *J. Chem. Phys.* **2003**, *119*, 1978–1985.
- (25) Di Stefano, M.; Rosi, M.; Sgamellotti, A.; Negri, F. Reactions of N⁺ Ions with Benzene: A Theoretical Study on the C₆NH₆⁺ Potential Energy Surface. *Chem. Phys.* **2004**, *302*, 295–308.
- (26) Parker, D. S. N.; Kaiser, R. I.; Kostko, O.; Troy, T. P.; Ahmed, M.; Sun, B.-J.; Chen, S.-H.; Chang, A. H. H. On the Formation of Pyridine in the Interstellar Medium. *Phys. Chem. Chem. Phys.* **2015**, *17*, 32000–32008.
- (27) Ricca, A.; Bauschlicher, C. W., Jr.; Bakes, E. L. O. A Computational Study of the Mechanisms for the Incorporation of a Nitrogen Atom into Polycyclic Aromatic Hydrocarbons in the Titan Haze. *Icarus* **2001**, *154*, 516–521.
- (28) Soorkia, S.; Taatjes, C. A.; Osborn, D. L.; Selby, T. M.; Trevitt, A. J.; Wilson, K. R.; Leone, S. R. Direct Detection of Pyridine Formation by the Reaction of CH (CD) with Pyrrole: A Ring Expansion Reaction. *Phys. Chem. Chem. Phys.* **2010**, *12*, 8750–8758.
- (29) McGuire, B. A.; Burkhardt, A. M.; Kalenskii, S.; Shingledecker, C. N.; Remijan, A. J.; Herbst, E.; McCarthy, M. C. Detection of the Aromatic Molecule Benzonitrile (c-C₆H₅CN) in the Interstellar Medium. *Science* **2018**, *359*, 202–205.

- (30) Jones, B. M.; Zhang, F.; Kaiser, R. I.; Jamal, A.; Mebel, A. M.; Cordiner, M. A.; Charnley, S. B. Formation of Benzene in the Interstellar Medium. *Proc. Natl. Acad. Sci. U. S. A.* **2011**, *108*, 452–457.
- (31) Cernicharo, J.; Heras, A. M.; Tielens, A. G. G. M.; Pardo, J. R.; Herpin, F.; Guelin, M.; Waters, L. B. F. M. Infrared Space Observatory's Discovery of C_4H_2 , C_6H_2 , and Benzene in CRL 618. *Astrophys. J.* **2001**, *546*, L123–L126.
- (32) Borden, W. T.; Gritsan, N. P.; Hadad, C. M.; Karney, W. L.; Kemnitz, C. R.; Platz, M. S. The Interplay of Theory and Experiment in the Study of Phenylnitrene. *Acc. Chem. Res.* **2000**, *33*, 765–771.
- (33) Karney, W. L.; Borden, W. T. Ab Initio Study of the Ring Expansion of Phenylnitrene and Comparison with the Ring Expansion of Phenylcarbene. *J. Am. Chem. Soc.* **1997**, *119*, 1378–1387.
- (34) Kemnitz, C. R.; Karney, W. L.; Borden, W. T. Why Are Nitrenes More Stable than Carbenes? An Ab Initio Study. *J. Am. Chem. Soc.* **1998**, *120*, 3499–3503.
- (35) Kvaskoff, D.; Luerssen, H.; Bednarek, P.; Wentrup, C. Phenylnitrene, Phenylcarbene, and Pyridylcarbenes. Rearrangements to Cyanocyclopentadiene and Fulvenallene. *J. Am. Chem. Soc.* **2014**, *136*, 15203–15214.
- (36) Winkler, M. Singlet-Triplet Energy Splitting and Excited States of Phenylnitrene. *J. Phys. Chem. A* **2008**, *112*, 8649–8653.
- (37) Nguyen, T. L.; Kim, G.-S.; Mebel, A. M.; Nguyen, M. T. A Theoretical Re-evaluation of the Heat of Formation of Phenylcarbene. *Chem. Phys. Lett.* **2001**, *349*, 571–577.
- (38) Bettinger, H. F.; Sander, W. Dehydrophenylnitrenes: Quartet versus Doublet States. *J. Am. Chem. Soc.* **2003**, *125*, 9726–9733.
- (39) Grote, D.; Sander, W. Photochemistry of Fluorinated 4-Iodophenylnitrenes: Matrix Isolation and Spectroscopic Characterization of Phenylnitrene-4-yls. *J. Org. Chem.* **2009**, *74*, 7370–7382.
- (40) Gu, X.; Guo, Y.; Zhang, F.; Mebel, A. M.; Kaiser, R. I. Reaction Dynamics of Carbon-Bearing Radicals in Circumstellar Envelopes of Carbon Stars. *Faraday Discuss.* **2006**, *133*, 245–275.
- (41) Gu, X.; Kaiser, R. I. Reaction Dynamics of Phenyl Radicals in Extreme Environments: A Crossed Molecular Beam Study. *Acc. Chem. Res.* **2009**, *42*, 290–302.
- (42) Guo, Y.; Gu, X.; Kawamura, E.; Kaiser, R. I. Design of a Modular and Versatile Interlock System for Ultrahigh Vacuum Machines: A Crossed Molecular Beam Setup as a Case Study. *Rev. Sci. Instrum.* **2006**, *77*, 034701.
- (43) Kaiser, R. I.; Maksyutenko, P.; Ennis, C.; Zhang, F.; Gu, X.; Krishtal, S. P.; Mebel, A. M.; Kostko, O.; Ahmed, M. Untangling the Chemical Evolution of Titan's Atmosphere and Surface - From Homogeneous to Heterogeneous Chemistry. *Faraday Discuss.* **2010**, *147*, 429–478.
- (44) Kaiser, R. I.; Suits, A. G. A High-Intensity, Pulsed Supersonic Carbon Source with $C(^3P)$ Kinetic Energies of 0.08–0.7 eV for Crossed Beam Experiments. *Rev. Sci. Instrum.* **1995**, *66*, 5405–5411.
- (45) Gu, X.; Guo, Y.; Kawamura, E.; Kaiser, R. I. Characteristics and Diagnostics of an Ultrahigh Vacuum Compatible Laser Ablation Source for Crossed Molecular Beam Experiments. *J. Vac. Sci. Technol., A* **2006**, *24*, 505–511.
- (46) Kaiser, R. I.; Stranges, D.; Lee, Y. T.; Suits, A. G. Neutral-Neutral Reactions in the Interstellar Medium. Part I. Formation of Carbon Hydride Radicals via Reaction of Carbon Atoms with Unsaturated Hydrocarbons. *Astrophys. J.* **1997**, *477*, 982–989.
- (47) Kaiser, R. I.; Balucani, N.; Charkin, D. O.; Mebel, A. M. A Crossed Beam and Ab Initio Study of the $C_2(X^1\Sigma_g^+/a^3\Pi_u) + C_2H_2(X^1\Sigma_g^+)$ Reactions. *Chem. Phys. Lett.* **2003**, *382*, 112–119.
- (48) Kaiser, R. I.; Mebel, A. M.; Chang, A. H. H.; Lin, S. H.; Lee, Y. T. Crossed-Beam Reaction of Carbon Atoms with Hydrocarbon Molecules. V. Chemical Dynamics of $n-C_4H_3$ Formation from Reaction of $C(^3P)$ with Allene, $H_2CCCH_2(X^1A_1)$. *J. Chem. Phys.* **1999**, *110*, 10330–10344.
- (49) Balucani, N.; Mebel, A. M.; Lee, Y. T.; Kaiser, R. I. A Combined Crossed Molecular Beam and Ab Initio Study of the Reactions $C_2(X^1\Sigma_g^+, a^3\Pi_u) + C_2H_4 \rightarrow n-C_4H_3(X^2A') + H(^2S_{1/2})$. *J. Phys. Chem. A* **2001**, *105*, 9813–9818.
- (50) Kaiser, R. I.; Sun, W.; Suits, A. G.; Lee, Y. T. Crossed Beam Reaction of Atomic Carbon, $C(^3P)$, with the Propargyl Radical, $C_3H_3(X^2B_2)$: Observation of Diacetylene, $C_4H_2(X^1\Sigma_g^+)$. *J. Chem. Phys.* **1997**, *107*, 8713–8716.
- (51) Kaiser, R. I.; Mebel, A. M.; Lee, Y. T. Chemical Dynamics of Cyclopropynylidyne ($c-C_3H$; X^2B_2) Formation from the Reaction of $C(^1D)$ with Acetylene, $C_2H_2(X^1\Sigma_g^+)$. *J. Chem. Phys.* **2001**, *114*, 231–239.
- (52) Vernon, M. F. *Molecular Beam Scattering*; University of California at Berkeley, Berkeley, CA, 1983.
- (53) Weiss, P. S. *The Reaction Dynamics of Electronically Excited Alkali Atoms with Simple Molecules*; University of California at Berkeley, Berkeley, CA, 1986.
- (54) Becke, A. D. Density-Functional Thermochemistry. III. The Role of Exact Exchange. *J. Chem. Phys.* **1993**, *98*, 5648–5652.
- (55) Lee, C.; Yang, W.; Parr, R. G. Development of the Colle-Salvetti Correlation-Energy Formula into a Functional of the Electron Density. *Phys. Rev. B: Condens. Matter Mater. Phys.* **1988**, *37*, 785–789.
- (56) Adler, T. B.; Knizia, G.; Werner, H.-J. A Simple and Efficient CCSD(T)-F12 Approximation. *J. Chem. Phys.* **2007**, *127*, 221106.
- (57) Knizia, G.; Adler, T. B.; Werner, H.-J. Simplified CCSD(T)-F12 Methods: Theory and Benchmarks. *J. Chem. Phys.* **2009**, *130*, 054104.
- (58) Dunning, T. H., Jr. Gaussian Basis Sets for Use in Correlated Molecular Calculations. I. The Atoms Boron through Neon and Hydrogen. *J. Chem. Phys.* **1989**, *90*, 1007–1023.
- (59) Zhang, J.; Valeev, E. F. Prediction of Reaction Barriers and Thermochemical Properties with Explicitly Correlated Coupled-Cluster Methods: A Basis Set Assessment. *J. Chem. Theory Comput.* **2012**, *8*, 3175–3186.
- (60) Celani, P.; Werner, H.-J. Multireference Perturbation Theory for Large Restricted and Selected Active Space Reference Wave Functions. *J. Chem. Phys.* **2000**, *112*, 5546–5557.
- (61) Shiozaki, T.; Gyorffy, W.; Celani, P.; Werner, H.-J. Communication: Extended Multi-State Complete Active Space Second-Order Perturbation Theory: Energy and Nuclear Gradients. *J. Chem. Phys.* **2011**, *135*, 081106.
- (62) Frisch, M. J.; Trucks, G. W.; Schlegel, H. B.; Scuseria, G. E.; Robb, M. A.; Cheeseman, J. R.; Scalmani, G.; Barone, V.; Mennucci, B.; Petersson, G. A., et al. *Gaussian 09*, Revision B.01; Gaussian Inc.: Wallingford CT, 2009.
- (63) Werner, H.-J.; Knowles, P. J.; Knizia, G.; Manby, F. R.; Schütz, M.; Celani, P.; Gyorffy, W.; Kats, D.; Korona, T.; Lindh, R., et al. *MOLPRO, A Package of Ab Initio Programs*, v 2010.1, 2010.
- (64) Robinson, P. J.; Holbrook, K. A. *Unimolecular Reactions*; Wiley: New York, 1972.
- (65) Eyring, H.; Lin, S. H.; Lin, S. M. *Basic Chemical Kinetics*; Wiley: New York, 1980.
- (66) Steinfeld, J.; Francisco, J.; Hase, W. *Chemical Kinetics and Dynamics*; Prentice Hall: Englewood Cliffs, NJ, 1989.
- (67) Kislov, V. V.; Nguyen, T. L.; Mebel, A. M.; Lin, S. H.; Smith, S. C. Photodissociation of Benzene under Collision-Free Conditions: An Ab Initio/Rice-Ramsperger-Kassel-Marcus Study. *J. Chem. Phys.* **2004**, *120*, 7008–7017.
- (68) Mebel, A. M.; Kaiser, R. I. Formation of Resonantly Stabilised Free Radicals via the Reactions of Atomic Carbon, Dicarbon, and Tricarbon with Unsaturated Hydrocarbons: Theory and Crossed Molecular Beams Experiments. *Int. Rev. Phys. Chem.* **2015**, *34*, 461–514.
- (69) Gu, X.; Guo, Y.; Mebel, A. M.; Kaiser, R. I. A Crossed Beam Investigation of the Reactions of Tricarbon Molecules, $C_3(X^1\Sigma_g^+)$, with Acetylene, $C_2H_2(X^1\Sigma_g^+)$, ethylene, $C_2H_4(X^1A_g)$, and Benzene, $C_6H_6(X^1A_g)$. *Chem. Phys. Lett.* **2007**, *449*, 44–52.
- (70) Zhang, F.; Kim, S.; Kaiser, R. I.; Mebel, A. M. Formation of the 1,3,5-Hexatriynyl Radical ($C_6H(X^2\Pi)$) via the Crossed Beams Reaction of Dicarbon ($C_2(X^1\Sigma_g^+/a^3\Pi_u)$), with Diacetylene ($C_4H_2(X^1\Sigma_g^+)$). *J. Phys. Chem. A* **2009**, *113*, 1210–1217.
- (71) Dangi, B. B.; Maity, S.; Kaiser, R. I.; Mebel, A. M. A Combined Crossed Beam and Ab Initio Investigation of the Gas Phase Reaction of Dicarbon Molecules (C_2 ; $X^1\Sigma_g^+/a^3\Pi_u$) with Propene (C_3H_6 ; X^1A'):

Identification of the Resonantly Stabilized Free Radicals 1- and 3-Vinylpropargyl. *J. Phys. Chem. A* **2013**, *117*, 11783–11793.

(72) Landera, A.; Mebel, A. M. Mechanisms of Formation of Nitrogen-Containing Polycyclic Aromatic Compounds in Low-Temperature Environments of Planetary Atmospheres: A Theoretical Study. *Faraday Discuss.* **2010**, *147*, 479–494.